SPE · AAPG · SEG
CCUS
Carbon Capture, Utilization, and Storage

CCUS: 4430850

Integrating Digital Rock Physics for Advanced Pore Scale Characterization of a Storage Complex With Implications in CO_2 Injection

William Apau Marfo*[1], William Ampomah[2], Tuhin Biswas[2], Tom Bratton [3]1. New Mexico Institute of Mining and Technology, 2. Petroleum Recovery Research Centre, 3. Tom Bratton LLC.

Abstract

This study advances pore-scale characterization of reservoir rocks by integrating Digital Rock Physics (DRP) to quantify pore geometry, grain fabric, and multiphase flow behavior. By linking pore structure to fluid transport, it evaluates how microscopic properties influence CO_2 injection dynamics and plume migration, improving prediction and monitoring of storage performance in the Entrada Sandstone of the San Juan Basin. High-resolution micro-CT imaging of Entrada sample was used to digitally segment pore spaces from mineral phases. Pore size distribution was quantified using granulometry and porosimetry, while Digital Routine and Special Core Analysis estimated porosity, connectivity, and multiphase flow parameters relevant to CO_2 injection. Percolation and permeability analyses were performed along principal flow directions, and laboratory core plug data (25.4 mm × 76.2 mm) were used to validate DRP results, ensuring robust CO_2 storage predictions. Pore-scale analysis revealed that pore throat distribution, grain arrangement, and mineral orientation are the primary controls on permeability, anisotropy, and connectivity, influencing fluid migration and trapping. These heterogeneities form preferential flow networks and barriers that govern CO_2 injectivity and long-term storage efficiency. Although porosity from DRP and experiments were nearly identical, simulated permeability was about six times higher, emphasizing the sensitivity of flow to microstructural features often missed by bulk measurements. Coordination number analysis showed strong correlation with permeability, where higher connectivity enhanced flow and CO_2 mobility. Relative permeability simulations indicated pronounced hysteresis, with wettability strongly impacting residual trapping and sweep efficiency. Archie's exponents (m, n) derived from resistivity curves improved water saturation estimation, enhancing CO_2 plume tracking and monitoring. Overall, this study demonstrates that pore-scale analysis provides critical insight into permeability, connectivity, and trapping efficiency by directly resolving microstructural features that

control CO_2 migration and storage, improving prediction accuracy and reliability of carbon capture and storage (CCS) site design.

Introduction

Geological carbon storage in deep saline aquifers and sandstone reservoirs is heavily dependent on the capacity of subsurface formations to securely and efficiently accommodate injected CO_2 while minimizing leakage risks and ensuring long-term trapping. Although traditional core analysis provides petrophysical properties such as porosity and permeability, it fails to truly resolve the microstructural controls (coordination number, pore throat size and distribution) that govern CO_2 injectivity, plume migration, residual trapping, and sweep efficiency (Ramandi et al., 2017; Saxena et al., 2017). These controls are ingrained in pore geometry, grain fabric, and pore connectivity, which operate at the micrometer scale and strongly influence multiphase flow behavior. Digital Rock Physics (DRP) has emerged as a transformative approach for pore-scale reservoir characterization, enabling direct numerical simulation of transport properties and multiphase flow behavior from high-resolution 3D rock images (Andrä et al., 2013; Mahmoud et al., 2023). By linking pore architecture to fluid transport mechanisms, DRP offers a physically consistent pathway to improve prediction and monitoring of CO_2 storage performance, particularly in heterogeneous formations (Sun et al., 2017). In this study, we combine DRP with hands-on lab work and detailed rock analysis to understand the Entrada Sandstone from the San Juan Basin. Our goal is straightforward: figure out how the microscopic features like the size and distribution of pore throats, the arrangement of grains, and how well the pores are connected affect the rock's ability to transport fluids in different directions, handle multiple fluids at once, and accommodate CO_2 injection.

Methodology

A high-resolution micro-CT scan of an Entrada Sandstone sample was used as the basis for constructing a digital rock model. The scanned volume had dimensions of 376 × 356 × 611 voxels with a voxel resolution of 5.146 μm, sufficient to capture pore throats and grain contacts relevant to multiphase flow. The workflow followed the “image and compute” paradigm, involving image preprocessing, AI-assisted segmentation of pore and mineral phases, and generation of a three-dimensional pore network (Figure 1). Digital Routine and Special Core Analysis modules were then applied to compute porosity, pore connectivity, pore size distribution, permeability, and multiphase flow parameters relevant to CO_2 injection and storage performance. Pore geometry was quantified using granulometry and porosimetry.

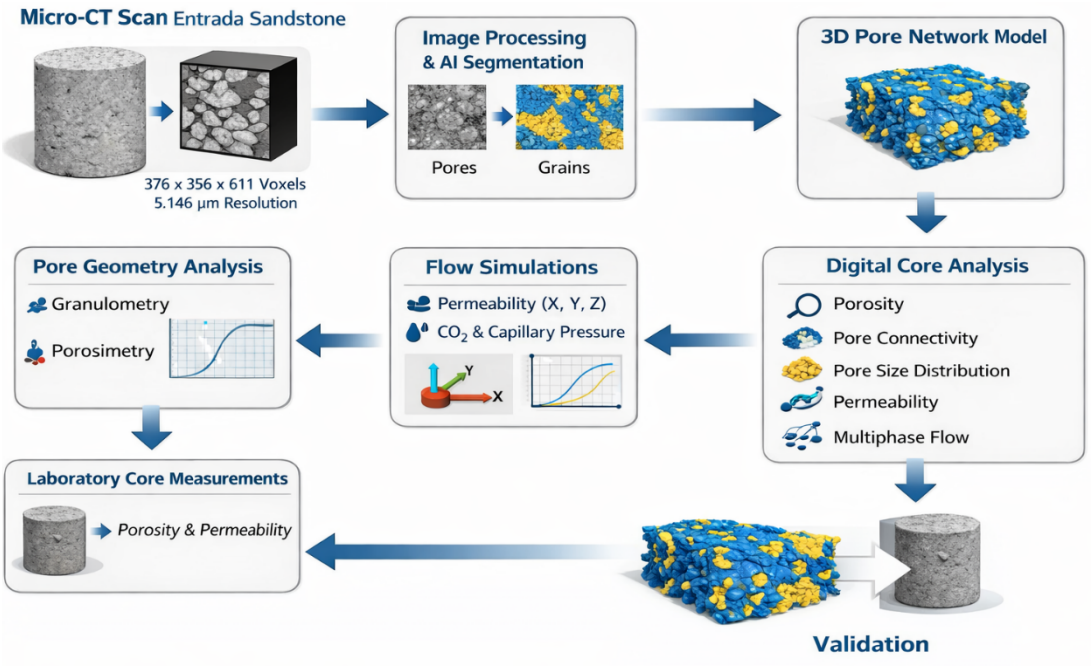

Figure 1 Methodological Framework for Pore-Scale Characterization Using Digital Rock Physics

Granulometry was employed to characterize the overall pore space geometry and mechanical relevance of pore sizes, while porosimetry emphasized hydraulically effective pore throats controlling fluid migration. Grain-scale morphological properties including grain shape, size distribution, coordination number, and orientation tensors were extracted to link rock fabric to anisotropy in flow and connectivity. Permeability simulations along the principal flow directions (X, Y, and Z) were performed to evaluate anisotropy and direction related transmissivity. To understand how CO_2 would flow, simulations were run to generate relative permeability curves and model capillary pressure (using MICP data) (Figure 3). These simulations showed how CO_2 gets trapped, how efficiently it spreads, and how capillary forces act. For ground truth, standard lab tests on a core plug were conducted, measuring its porosity and permeability. These traditional measurements served as a check for the digital rock models, which helped in understanding how small-scale pore data can be scaled up to predict reservoir-wide behavior.

Results

The DRP analysis revealed an overall porosity of 17.66%, with more than 99% of this porosity classified as open (17.59%) and hydraulically connected (Figure 2A). Through pores (17.57%) dominated the pore system, revealing that majority of the pore volume contributes to effective fluid transport (Figure 4). Closed and dead-end pores accounted for less than 0.1% of the total porosity which had little impact on storage and transmissibility (Figure 4). The highly connected through pores is favorable for CO_2 injectivity and plume propagation, as it reduces the likelihood of isolated, non-communicating pore clusters that could impede flow or trap CO_2 in inaccessible regions. Granulometry showed a broad pore size distribution with dominant pore diameters in the range of 20–30 µm and a long tail toward larger pores, reflecting the overall pore architecture (Figure 2C). However, porosimetry revealed a narrower distribution with characteristic pore throats centered around a range of 13–18 µm, revealing pore constrictions that directly control fluid flow.

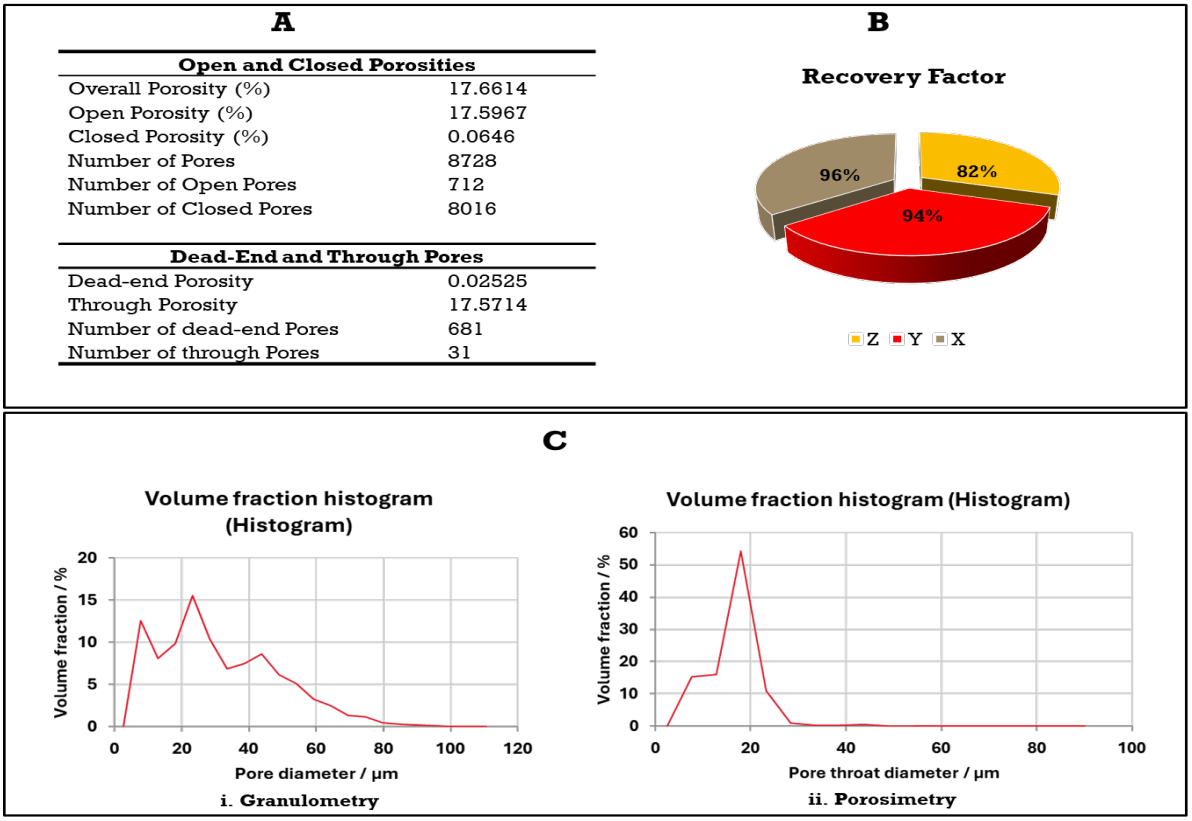

Figure 2 (A) Calculated porosity and pore connectivity from Digital Rock Physics analysis, (B) recovery factor derived from multiphase flow simulations, and (C) pore size distributions obtained from porosimetry (right) and granulometry (left) simulations.

This observed difference highlights a fundamental principle for CO_2 storage. In that, total pore volume defines the storage capacity, whereas injectivity and plume dynamics are constrained by a more limited network of effective pore throats. A complete assessment of storage performance, therefore, requires integrating both volumetric and dynamic pore-scale characteristics. Permeability simulations revealed moderate anisotropy with values of 739 mD, 690 mD and 595 mD in the X, Y and Z directions respectively (Table 1). The calculated arithmetic mean of 674 mD indicates a high transmissibility at the pore scale. This anisotropy is directly linked to grain orientation and pore alignment rather than sedimentary layering, demonstrating that pore-scale fabric can impose directional flow behavior even in macroscopically homogeneous sandstones. For CO_2 injection, this implies preferential plume migration along high-connectivity directions and more restricted vertical movement, a favorable condition for lateral plume spreading and vertical containment. Relative permeability simulations revealed recovery factors of approximately 96%, 94%, and 82% in the X, Y, and Z directions, respectively (Figure 2B). The lowest residual oil saturations occurred in the X direction, indicating the most efficient displacement and flow continuity, while the Z direction exhibited the highest residual saturation, reflecting increased trapping and reduced flow efficiency. These results are directly relevant to CO_2 storage, as they indicate that pore-scale heterogeneity controls both injectivity and residual trapping. Directions with higher residual saturation are more likely to enhance capillary trapping of CO_2, improving storage security, while well-connected directions facilitate plume migration and pressure dissipation. The DRP derived porosity showed excellent agreement with laboratory and thin section estimates, confirming the robustness of the segmentation and digital reconstruction. However, DRP simulated permeability was six times higher than laboratory values. The difference in permeabilities reflects scale effects: laboratory permeability integrates macroscopic heterogeneities such as laminations and continuously cemented zones, whereas

DRP captures the intrinsic transmissivity of a homogeneous sub-volume at the micro scale. Rather than indicating error, this contrast highlights the complementary nature of DRP and laboratory methods in characterizing both fundamental pore-scale physics and field-scale effective properties.

Discussion

The results demonstrate that pore-scale architecture exerts a first-order control on CO_2 injection dynamics and storage efficiency. Pore throat distribution governs injectivity and plume mobility, while pore connectivity and pore coordination number influence the continuity of flow paths and pressure dissipation. Grain fabric, expressed through orientation tensors and grain shape distributions, directly translates into permeability anisotropy and directional sweep efficiency. Importantly, the observed anisotropy suggests that even in relatively uniform sandstones, plume migration will be directionally biased, an effect that must be taken into account when dealing with storage simulations. Furthermore, the presence of both connected flow paths (through pores) and zones of restricted flow (closed pores) promotes a combination of structural, residual, and capillary trapping mechanisms, enhancing long-term CO_2 immobilization. The disparity between DRP and laboratory permeability highlights the need for upscaling strategies that reconcile pore-scale predictions with core scale and reservoir scale heterogeneity. The DRP analysis does not replace conventional measurements but rather adds additional insight which helps to resolve the physical mechanisms that govern the bulk rock fabric behavior.

Conclusions

Integrating Digital Rock Physics with traditional methods provides a robust framework for understanding CO_2 storage performance. This Entrada Sandstone study reveals that pore-scale heterogeneity and anisotropy critically control flow and trapping at the micro-scale, where formation properties are assumed uniform. These findings highlight the essential role of pore-scale insights in CCS site evaluation and simulation.

References

Andrä, H., Combaret, N., Dvorkin, J., Glatt, E., Han, J., Kabel, M., Keehm, Y., Krzikalla, F., Lee, M., Madonna, C., Marsh, M., Mukerji, T., Saenger, E.H., Sain, R., Saxena, N., Ricker, S., Wiegmann, A., and Zhan, X. 2013. Digital Rock Physics Benchmarks—Part I: Imaging and Segmentation. *Computers & Geosciences* 50: 25–32. http://dx.doi.org/10.1016/j.cageo.2012.09.005.

Mahmoud, A., Gajbhiye, R., Li, J., Dvorkin, J., Hussaini, S.R., and AlMukainah, H.S. 2023. Digital Rock Physics (DRP) Workflow to Assess Reservoir Flow Characteristics. *Arabian Journal of Geosciences* 16 (4): 248. http://dx.doi.org/10.1007/s12517-023-11314-3.

Ramandi, H.L., Mostaghimi, P., and Armstrong, R.T. 2017. Digital Rock Analysis for Accurate Prediction of Fractured Media Permeability. *Journal of Hydrology* 554: 817–826. http://dx.doi.org/10.1016/j.jhydrol.2016.08.029.

Saxena, N., Hofmann, R., Alpak, F.O., Dietderich, J., Hunter, S., and Day-Stirrat, R.J. 2017. Effect of Image Segmentation and Voxel Size on Micro-CT Computed Effective Transport and Elastic Properties. *Marine and Petroleum Geology* 86: 972–990. http://dx.doi.org/10.1016/j.marpetgeo.2017.07.004.

Saxena, N., Hows, A., Hofmann, R., Alpak, F.O., Freeman, J., Hunter, S., and Appel, M. 2018.

Imaging and Computational Considerations for Image-Computed Permeability: Operating Envelope of Digital Rock Physics. *Advances in Water Resources* 116: 127–144. http://dx.doi.org/10.1016/j.advwatres.2018.04.001.

Saxena, N. and Mavko, G. 2016. Estimating Elastic Moduli of Rocks from Thin Sections: Digital Rock Study of 3D Properties from 2D Images. *Computers & Geosciences* 88: 9–21. http://dx.doi.org/10.1016/j.cageo.2015.12.008.

Sun, H., Vega, S., and Tao, G. 2017. Analysis of Heterogeneity and Permeability Anisotropy in Carbonate Rock Samples Using Digital Rock Physics. *Journal of Petroleum Science and Engineering* 156: 419–429. http://dx.doi.org/10.1016/j.petrol.2017.06.002.

APPENDIX

Table 1 Comparison of core-plug porosity and permeability measurements with porosity and permeability predicted from Digital Rock Physics analysis.

SAMPLE	LABORATORY MEASUREMENTS		DRP MEASUREMENTS						
	Porosity (%)	Permeability (mD)	Porosity	Permeability (mD)			Average Permeability (mD)		
				X	Y	Z	Arithmetic	Harmonic	Geometric
Sandstone (Entrada)	18	104.30	17.66	739	690	595	674	669	672

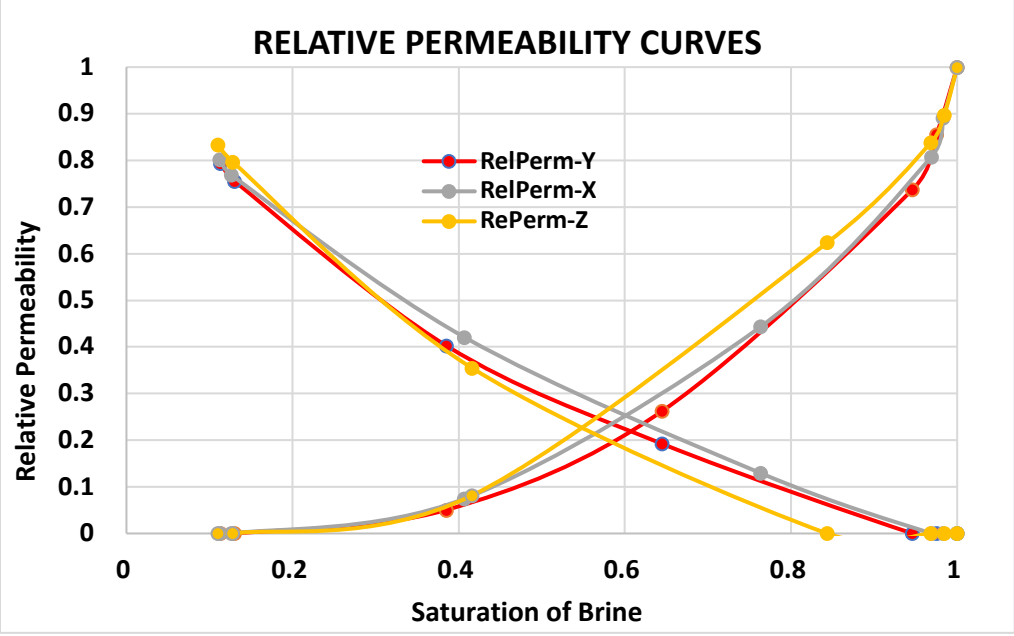

Figure 3 Directional relative permeability curves from Digital Rock Physics multiphase simulations for the X, Y, and Z principal flow directions.

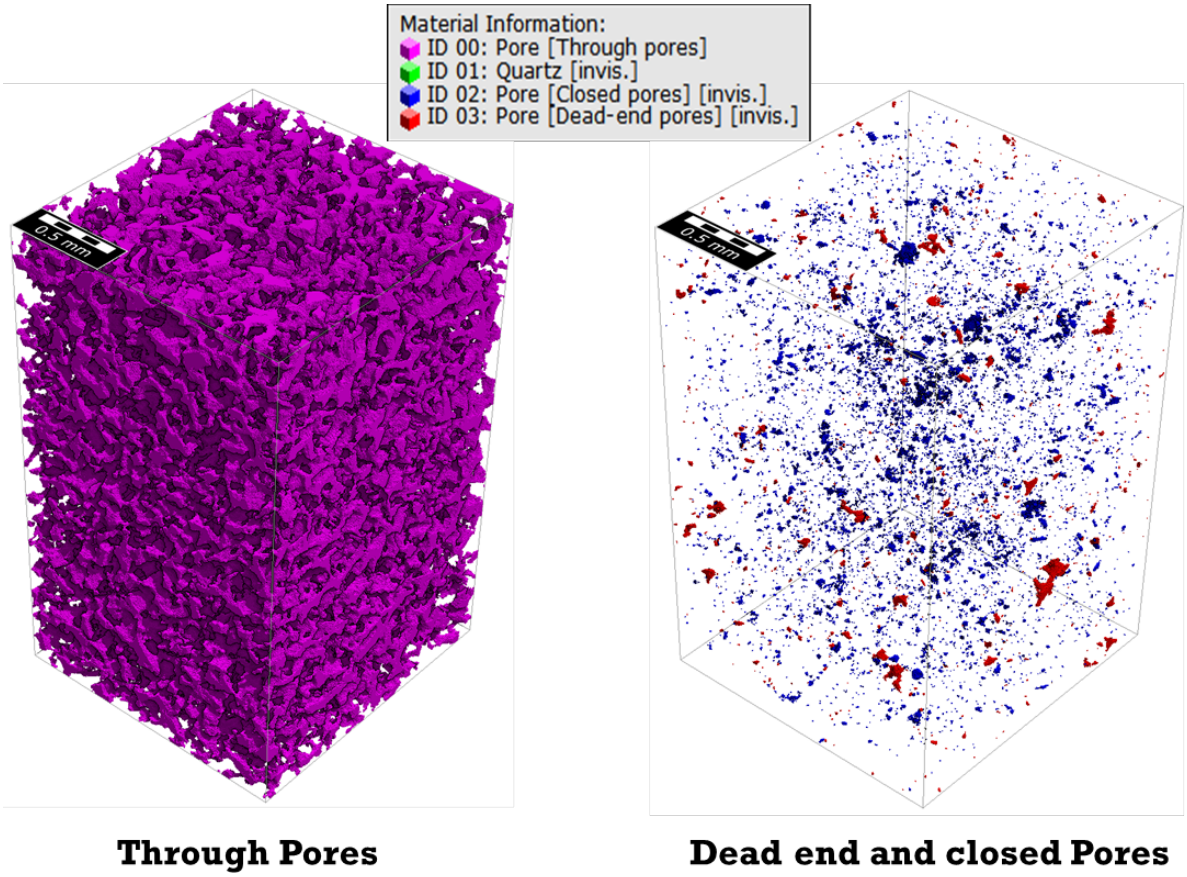

Figure 4 Three-dimensional visualization of pore connectivity from Digital Rock Physics analysis, showing (left) through pores forming the effective flow network and (right) the spatial distribution of dead-end and closed pores.

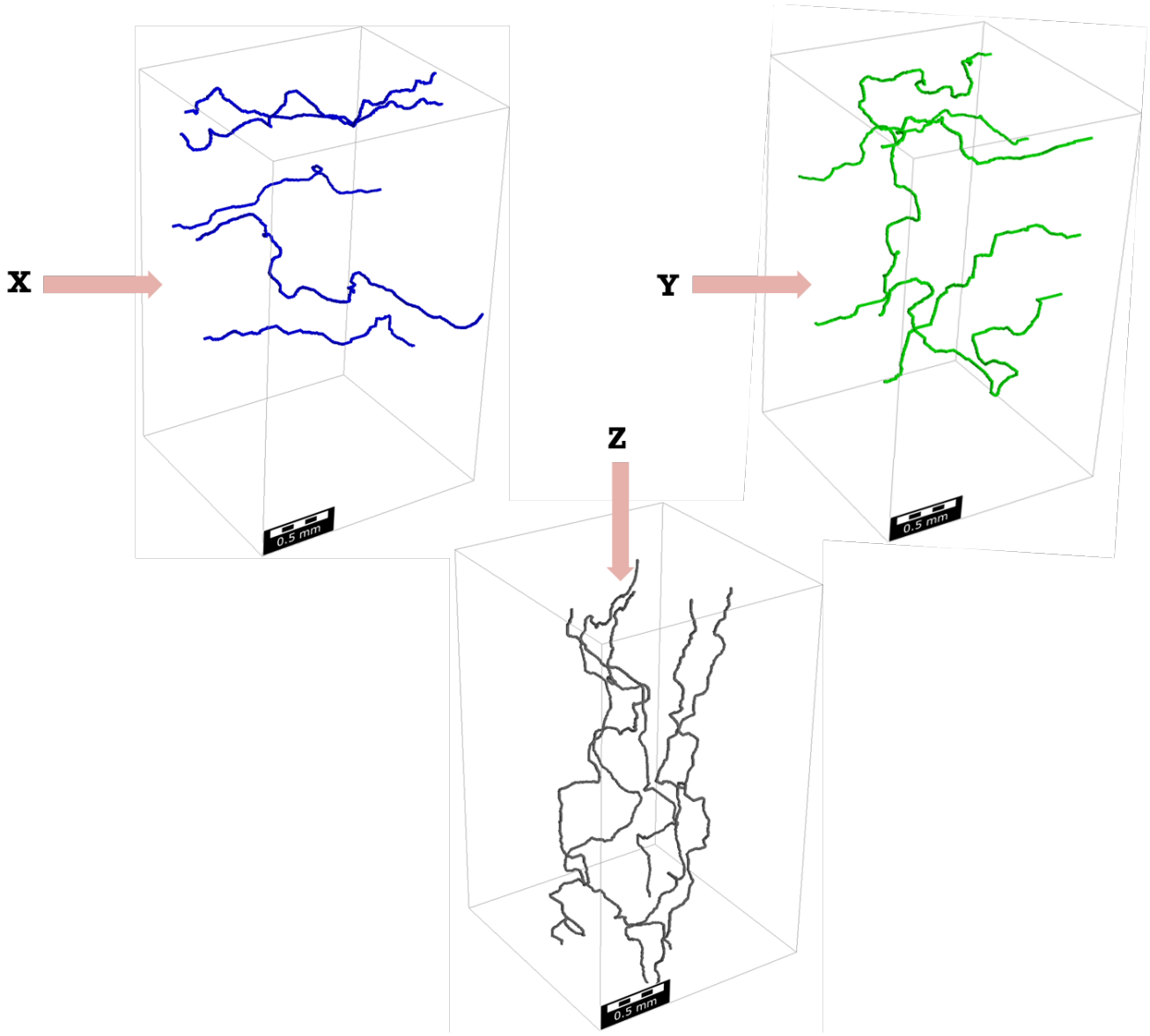

Figure 5 Three-dimensional percolation paths showing preferential pore connectivity and flow pathways along the principal X, Y, and Z directions.